

Particle-laden pipe flows at high volume fractions show transition without puffs

Hogendoorn, Willian; Poelma, Christian

DOI

[10.1103/PhysRevLett.121.194501](https://doi.org/10.1103/PhysRevLett.121.194501)

Publication date

2018

Document Version

Final published version

Published in

Physical Review Letters

Citation (APA)

Hogendoorn, W., & Poelma, C. (2018). Particle-laden pipe flows at high volume fractions show transition without puffs. *Physical Review Letters*, 121(19), Article 194501 .
<https://doi.org/10.1103/PhysRevLett.121.194501>

Important note

To cite this publication, please use the final published version (if applicable).
Please check the document version above.

Copyright

Other than for strictly personal use, it is not permitted to download, forward or distribute the text or part of it, without the consent of the author(s) and/or copyright holder(s), unless the work is under an open content license such as Creative Commons.

Takedown policy

Please contact us and provide details if you believe this document breaches copyrights.
We will remove access to the work immediately and investigate your claim.

Particle-Laden Pipe Flows at High Volume Fractions Show Transition Without Puffs

William Hogendoorn* and Christian Poelma†

Delft University of Technology, Multiphase Systems (3ME-P&E), 2628 CA Delft, The Netherlands



(Received 26 July 2018; published 6 November 2018)

Using ultrasound imaging velocimetry, we are able to present unique insight in transitional particle-laden flows. Together with a Moody diagram of time-averaged properties, we demonstrate that the laminar-turbulent transition behavior at high volume fractions is distinct from the single-phase case and cases with low volume fractions. For low volume fractions, a sharp transition is found with the presence of turbulent puffs, similar to the single-phase case. Seemingly, particles in this regime trigger subcritical transition. For high volume fractions a smooth transition is discovered without turbulent puffs in the transition regime. For this regime, particles cause a supercritical transition.

DOI: [10.1103/PhysRevLett.121.194501](https://doi.org/10.1103/PhysRevLett.121.194501)

In 1883, Reynolds performed experiments on laminar-turbulent flow transition that remain relevant to this very day [1]. Despite considerable research efforts, many aspects of this phenomenon remain unknown. Since pipe flow is linearly stable, finite amplitude perturbations are required to trigger the flow to a turbulent state [2–4]. Depending on the amplitude of the perturbation, the onset to turbulence is found to vary [5]. This onset is usually expressed with the Reynolds number ($Re = U_b D / \nu$; U_b is the bulk flow velocity, D the pipe diameter, and ν the kinematic viscosity), which typically ranges from 1700 to 2300 [2,6]. The onset of transition starts with the appearance of turbulent “puffs.” Depending on the Reynolds number, puffs typically extend 20–30 diameters along the pipe [3,7] and become more numerous with an increasing Reynolds number. Initially, they have a finite lifetime [8,9]. For Reynolds numbers above approximately 2040 they split and grow, leading to sustained turbulence [6].

The transition behavior changes significantly when particles are added [10]. Particle-laden flows are of major interest because of their environmental and industrial applications. Recent research relies predominantly on numerical simulations (e.g., [11,12]), because the opaque nature of these flows precludes conventional experimental techniques. However, we show in this Letter that ultrasound-based techniques can provide unprecedented insight in these flows.

A seminal study of the influence of particles on laminar-turbulent transition was performed by Matas *et al.* [10]. Based on low-frequency variations in the pressure drop, they were able to detect turbulent puffs and by that the critical (i.e., transition) Reynolds number, Re_c . For particles bigger than $D/65$ the value of Re_c was found to be a nonmonotonic function of the particle volume fraction (ϕ): initially, for increasing volume fractions, Re_c decreased. However, for larger volume fractions Re_c increased with

increasing ϕ and the transition is eventually delayed compared to single-phase flows.

Yu *et al.* [11] studied the same experiment numerically. Having access to the velocity fields, the authors pointed out that the flow was not smooth, even in the laminar regime. This was attributed to local disturbances by the particles. This made it difficult to judge whether the flow is laminar or turbulent. To capture Re_c they used the energy of the streamwise velocity fluctuation as indicator. For a critical value of this energy, large-scale vortices (i.e., similar in size as the particles) start to appear, indicating that the flow is turbulent.

Further progress was made in a recent study by Lashgari *et al.* [12]. Although they used a channel flow configuration, the results are relevant for pipe flow as well, despite the presence of secondary flow patterns in channels [13]. Based on the stress budget, the authors found three different regimes as functions of Re and volume fraction: a laminar-like (viscous stress dominated), turbulentlike (Reynolds stress dominated), and inertial shear-thickening (particle stress dominated) regime. For low volume fractions they found a sharp laminar-turbulent transition, i.e., a fairly sudden increase in flow resistance with increasing Re . For higher volume fractions this was no longer the case. They conclude that inertial shear thickening and coherent turbulence coexists with different relevance. The computationally intensive nature of these simulations prohibits studying an extensive parameter range, especially since the transition regime requires a very long data series for convergence [8].

In this Letter we show that laminar-turbulent transition behavior for higher volume fractions in pipe flow is different than transition at lower volume fractions. Through unique experimental velocity data, we refine the transition scenarios in particle-laden flows and explain the observed flow resistance curves. A sharp transition is found for low volume fractions, with the presence of turbulent puffs in the

transition region. For higher volume fractions a gradual transition is observed; turbulent puffs appear to be absent.

Experiments are performed in a glass pipe setup with an inner diameter of 10 ± 0.01 mm. Water is used as the continuous phase and polystyrene particles (Synthos; diameter $d = 530$ μm ; $D/d = 19$; density $\rho = 1.032$ kg/L) are used as the dispersed phase. Salt (Na_2SO_4) is added to the water to make the particles neutrally buoyant. To avoid perturbations by a pump, the flow is gravity driven. The outflow is fed back to a feeding tank using a set of peristaltic pumps. This tank is equipped with an overflow to maintain a precise, fixed pressure head. The height of the tank is changed to vary Re , in random order. A converging inlet chamber is used to ensure smooth inflow conditions. After this inlet chamber a ring (inner diameter of 8.5 mm) is placed to trip the flow. The pipe length (L) after the ring is $310D$. The pressure drop (ΔP) is measured between $125D$ to $250D$ downstream using a Validyne DP15. Pressure data were averaged for at least 30 seconds, ensuring convergence.

Velocity data is obtained $270D$ downstream using ultrasound imaging velocimetry (UIV; [14]), based on a SonixTOUCH echography system with an L14-5/38 linear probe. UIV provides time-dependent velocity fields within a thin slice. This is achieved by local cross-correlation of tracer particle images obtained by echography. Here the slice is aligned with the streamwise and radial axes. With the hardware and processing settings used, the spacing between vectors in the radial and streamwise direction is 0.45 mm and 4.8 mm, respectively; the thickness of the slice is 2 mm. To improve the signal-to-noise ratio the local cross-correlation is determined using results of a sliding average of ten subsequent ultrasound images. This introduces temporal filtering: the effective temporal resolution reduces from 260 (the image frame rate) to 26 Hz, equivalent to a spatial resolution of $1.5D$ at a typical centerline velocity of 0.4 m/s. This relatively coarse resolution is still much smaller than the typical puff length of $20\text{--}30D$, which means that turbulent puffs can be detected. This is validated with a single-phase reference measurement in both a laminar and turbulent state, using tracer particles with a diameter of 56 μm . All acquisition and processing settings are kept constant. For the laminar case, a root-mean-square variation of 0.8% (u_{rms}/U_c) is found. This variation comprises measurement uncertainty and physical variations in the flow; the value serves as reference value for undisturbed, laminar flows.

The temperature is measured in the downstream collection chamber and the viscosity of the water is corrected accordingly. The volumetric flow rate is determined with an accuracy better than 0.5% by measuring the time it takes to collect a given volume of suspension from the outflow. A single-phase system characterization, without ring, confirms that the setup is disturbance free up to at least $\text{Re} \approx 4000$: in this range the Darcy friction factor, i.e., the

dimensionless pressure difference $f \equiv \Delta P / (\frac{1}{2}\rho U_b^2 L/D)$, was found to agree with Poiseuille's law, $f = 64/\text{Re}$.

Particles are added in steps, from 0% to 20% weight (as the particles are neutrally buoyant, volume fraction equals weight fraction). After the measurements, a sample of the suspension was collected and weighted. Rinsing, drying and weighing the particles gave an uncertainty in volume fraction at the highest load of 1%. The dynamic viscosity of the suspension ($\mu = \nu\rho$) is corrected using Eilers's model [15], given by the following:

$$\frac{\mu}{\mu_0} = \left(1 + 1.25 \frac{\phi}{1 - \phi/0.64} \right)^2, \quad (1)$$

with μ_0 as the single-phase viscosity. With this empirical relation, the viscosity diverges at high volume fractions, when the systems approaches the jamming transition. However, for the volume fractions used here ($\phi \leq 20\%$), there is a good agreement with experimental data [16]. This is also evident from the fact that using this correction all laminar(like) results collapse on the $64/\text{Re}$ curve.

Figure 1(a) shows the transition behavior for five selected cases. The friction factor is shown as function of Reynolds number, commonly known as a Moody diagram. The friction factor for Poiseuille flow, $64/\text{Re}$, is plotted as a continuous line. The single-phase transition curve is presented as well ("0%") and a transition at $\text{Re}_c \approx 2000$ is found, a value specific for this facility and perturbation. In panel (b) of Fig. 1, all experiments are shown in an alternative manner.

From both panels three different observations can be made: in the first place, Re_c decreases for increasing volume fraction. In panel (b), the dashed curve (" $L \rightarrow T$ ") indicates where the friction factor exceeds Poiseuille's law by 10%, a pragmatic way to describe the onset of transition. A minimum ($\text{Re}_c \approx 1350$) is found for $\phi \approx 8\%$. This is in agreement with the observations of Matas *et al.* [10] and Yu *et al.* [11].

Second, Re_c does not increase for higher volume fractions. This is in contrast to what was reported by Matas *et al.* [10], yet this is likely due to their method of determining the flow state (using the spectrum of pressure fluctuations). Here, we observe a change in transition behavior in the sense that there is no sharp transition anymore. This can be seen for the $\phi = 17.5\%$ case in Fig. 1, where the local minimum has disappeared. In panel (b), the solid curve (" $f_{\text{local max}}$ ") indicates the local maximum in the friction factor curve (again a pragmatic way of describing the end of transition). No local maximum can be observed for cases with $\phi > 15\%$; i.e., the friction factor monotonically decreases with increasing Re .

In the third place, a drag increase is found for particle-laden pipe flow in the turbulent regime. This drag increase is found to be a function of volume fraction, but seemingly there is a maximum drag increase of 17% for $\phi = 10\%$

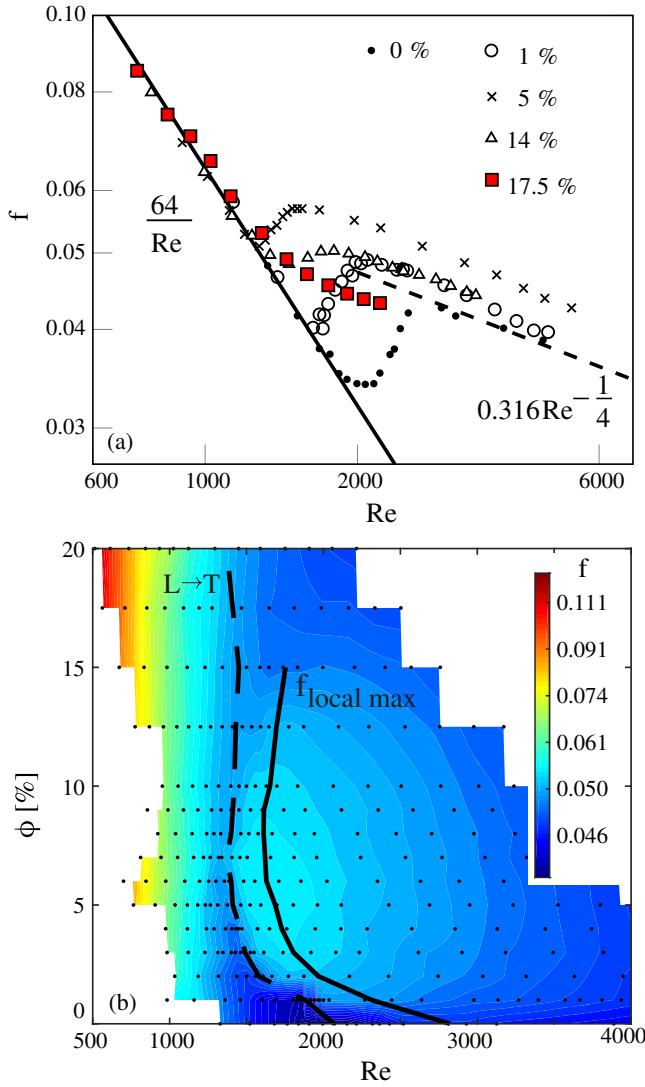


FIG. 1. The friction factor as function of Reynolds number (panel a, selected cases) and as function of Reynolds number and volume fraction (panel b, where each marker represents a measurement).

(corrected with Eilers’s viscosity fit) with respect to Blasius’s friction law for turbulent flows (dashed line, $f = 0.316Re^{-1/4}$). For $\phi > 10\%$ this drag increase is reduced as can be seen in Fig. 1(a) in the 14% transition

curve. The drag increase for cases up to $\phi = 10\%$ are in line with results from numerical simulations [17], once adjusted for geometry differences (channel versus pipe).

To investigate this change in laminar-turbulent transition in more detail, UIV is applied to two representative cases: $\phi = 1\%$ and $\phi = 14\%$.

The velocity measurements here rely on the dispersed phase as tracers. Their response time is sufficiently small, as they are neutrally buoyant. However, the particles are relatively large and can thus only follow turbulent eddies of equal or larger size. This means that the suspension behavior can only be inferred in a semiquantitative way, as flow features smaller than a particle diameter are lost.

In Fig. 2, representative visualizations of the radial (v) velocities for various Reynolds numbers are shown for the case of $\phi = 1\%$. Each panel is constructed as a time series of the radial profile of the radial velocity component. Using Taylor’s hypothesis, this can qualitatively be interpreted as a spatial representation of the flow in the pipe. Recently, Cerbus *et al.* [18] confirmed that the friction factor in the transition regime is a combination of the laminar ($64/Re$, in between puffs) and a turbulent friction factor (for the puffs):

$$f = \gamma f_{puffs} + (1 - \gamma) f_{lam}, \quad (2)$$

where γ , the intermittency, represents the fraction of flow corresponding to puffs. Since the friction factor for each Reynolds number is known, γ can be determined. Because there is a drag increase in the turbulent region (for $\phi = 1\%$ a drag increase of 4% is found), a slightly different multiplier for Blasius’s law is used (0.329 instead of 0.316) based on a fit to our data. The resulting intermittency values are shown in the Figure. The values match with a visual inspection of the flow structure and pressure signals.

For $Re = 1375$, laminarlike flow is observed. By “laminarlike,” we imply that the friction factor is on the $64/Re$ curve, as long as Re is based on the effective viscosity [Eq. (1)]. A continuous variation is apparent in the velocity data, which can be attributed to fluctuations introduced by the particles. A variation u_{rms}/U_c of 3.0% is found. These fluctuations are associated with the increased effective viscosity. The next three panels are in the transition region,

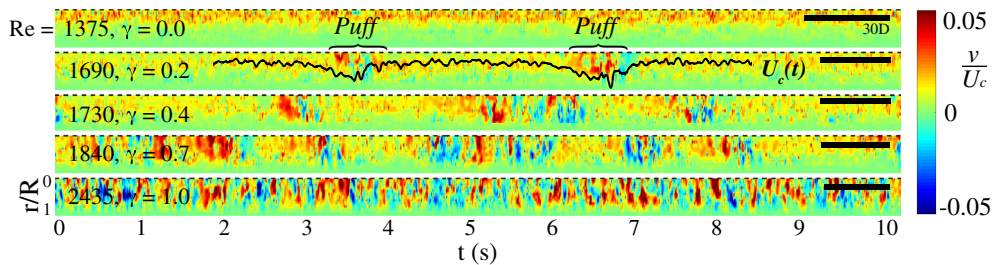


FIG. 2. Radial (v) velocity data as function of time for five different Reynolds numbers for $\phi = 1\%$. The intermittency γ represents the fraction of puffs and is obtained from the pressure drop signal. The velocity data are normalized using the centerline velocity. A bar of length $30D$ (based on the averaged centerline velocity for each Re) is shown in the top right corner for each panel. Only the top half of the pipe is shown; the radial positions (r) are normalized with the pipe radius R .

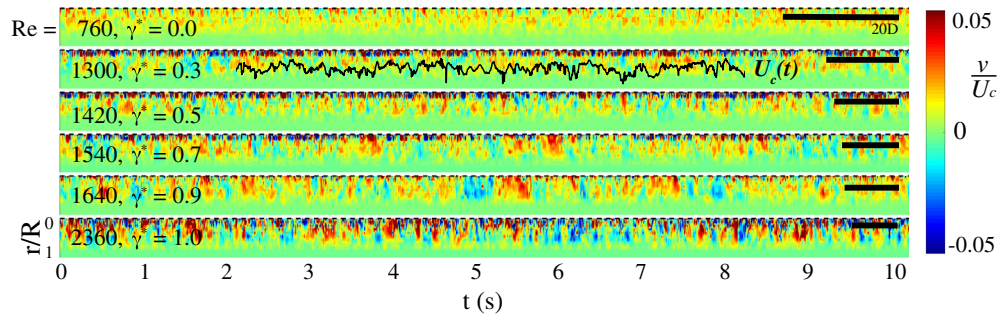


FIG. 3. Radial (v) velocity data as function of time for six different Reynolds numbers for $\phi = 14\%$.

corresponding to $\gamma = 0.2$, 0.4 , and 0.7 , respectively. In these panels, puffs can be identified as confined regions with significant fluctuations. The length scale for these puffs is found to be $\mathcal{O}(30D)$, which is in agreement with results for puffs in single-phase flow [3,7]. For $\gamma = 0.2$ the time-dependent centerline velocity is superimposed (in arbitrary scaling), showing the characteristic sawtooth shape around both puffs [8]. Seemingly, for this particle volume fraction the physical mechanism is not changed significantly. For the final panel, with $\gamma = 1$, the flow is found to be fully turbulent, as can be seen from the continuously fluctuating velocity component. From these observations, it is clear that a particle-laden flow can exhibit a traditional laminar to turbulent transition; the main effect of the particles is an earlier onset, as $\text{Re}_c \approx 2000$ decreases to $\text{Re}_c \approx 1700$ for $\phi = 1\%$.

The second case investigated is the flow with $\phi = 14\%$. In Fig. 3, representative examples of the radial velocity component are shown for six different Reynolds numbers. For each Re , the value of γ^* is reported. As will be discussed later, this parameter can no longer be interpreted as intermittency, hence the asterisk. For $\phi = 14\%$, a drag increase of 8% is found in the turbulent region. Based on this, the constant in Blasius's equation is changed to 0.341 and the values of γ^* are again determined using Eq. (2). For the laminarlike case ($\text{Re} = 760$) a variation of 10.3% (u_{rms}/U_c) is found, as a result of the presence of the particles. Despite the “laminar” nature, we can again observe structures. These extend in the radial direction, which confirms that they are physical fluctuations rather than measurement errors smeared out by the sliding average (which only operates in the temporal direction).

The next four sets are captured in the transition region, for $\gamma^* = 0.3$, 0.5 , 0.7 , and 0.9 respectively. However, from the radial velocity data no clear puffs can be distinguished, which is in contrast to the previous case with $\phi = 1\%$. In all signals, continuous radial velocity fluctuations are present, which are increasing in intensity as a function of Reynolds number. For case $\gamma^* = 0.3$, the centerline velocity is shown, which shows no recognizable puff signatures. This indicates that the transition behavior at high volume fractions is different from transition behavior of a single-phase flow or

dilute suspensions. The intermittency parameter γ^* reported earlier does here not represent a fraction of puffs, but only the relative position between (extrapolated) laminar and turbulent friction factor curves. For $\phi > 15\%$ it is no longer possible to define a γ^* , which is indicative of the absence of distinct, coexisting laminar (low friction) and turbulent (higher friction) states.

These observations raise the question what happens in an intermediate case. A UIV dataset for the case $\phi = 8\%$ is analyzed, which has a friction factor curve in between $\phi = 1\%$ and 14% (Fig. 1). In the transition region, weak large-scale structures can be seen; however, they are not as distinct as the puffs shown in the case for $\phi = 1\%$. The flow in between these structures has an increasing fluctuation intensity due to the particles. This indicates that there is a gradual change from the transition behavior found for $\phi = 1\%$ to the behavior found for $\phi = 14\%$. With increasing concentration, puffs become weaker with respect to the surrounding flow, which exhibits more intense fluctuations.

An explanation of the observed behavior relies on two mechanisms: the (local) disturbances introduced by the particles may interfere with the self-sustaining nature [19] of puffs. Splitting and growth of puffs has been identified as a key mechanism in the transition to turbulence [6]. Absence of puffs, however, therefore suggests that an alternative route must be present, as the flow clearly becomes turbulent. This second route is again rooted in the local disturbances by the particles: for single-phase and dilute systems, flow disturbances are small and lead to a subcritical transition (evident in the coexistence of laminar and turbulent regions). On the other hand, in the densely laden cases, the disturbances can no longer be considered to be small and lead to a supercritical transition. The disturbances grow globally, with increasing Reynolds number, towards a fully turbulent flow.

In summary, we show that the transition behavior for particle-laden flows at high volume fraction is distinctly different from the transition of single-phase or dilute particle-laden flows. For low volume fractions, particles trigger earlier (subcritical) transition, as the particles introduce disturbances to the flow. From the friction curve a sharp transition is observed. For higher volume fractions,

transition behavior is found to be distinctly different. In the Moody diagram a gradual transition is observed. Investigating the velocity field with UIV shows that there are no turbulent puffs in the transition region for the high volume fraction case, contrary to the dilute case. A description in terms of a supercritical transition is more appropriate. This also suggests that the friction factor curve for densely laden flows will be more universal than that for single-phase flows, for which the transition region is notoriously unpredictable.

This work is funded by the ERC Consolidator Grant No. 725183 “OpaqueFlows.”

*W.J.Hogendoorn@tudelft.nl

†C.Poelma@tudelft.nl

- [1] O. Reynolds, *Phil. Trans. R. Soc. London* **174**, 935 (1883).
- [2] R. Kerswell, *Nonlinearity* **18**, R17 (2005).
- [3] B. Eckhardt, T. M. Schneider, B. Hof, and J. Westerweel, *Annu. Rev. Fluid Mech.* **39**, 447 (2007).
- [4] P. G. Drazin and W. H. Reid, *Hydrodynamic Stability* (Cambridge University Press, Cambridge, England, 2004).
- [5] B. Hof, A. Juel, and T. Mullin, *Phys. Rev. Lett.* **91**, 244502 (2003).
- [6] K. Avila, D. Moxey, A. de Lozar, M. Avila, D. Barkley, and B. Hof, *Science* **333**, 192 (2011).
- [7] I. Wygnanski and F. Champagne, *J. Fluid Mech.* **59**, 281 (1973).
- [8] D. J. Kuik, C. Poelma, and J. Westerweel, *J. Fluid Mech.* **645**, 529 (2010).
- [9] B. Hof, J. Westerweel, T. M. Schneider, and B. Eckhardt, *Nature (London)* **443**, 59 (2006).
- [10] J.-P. Matas, J. F. Morris, and E. Guazzelli, *Phys. Rev. Lett.* **90**, 014501 (2003).
- [11] Z. Yu, T. Wu, X. Shao, and J. Lin, *Phys. Fluids* **25**, 043305 (2013).
- [12] I. Lashgari, F. Picano, W.-P. Breugem, and L. Brandt, *Phys. Rev. Lett.* **113**, 254502 (2014).
- [13] H. Schlichting, *Boundary-Layer Theorie* (McGraw-Hill, New York, 1979).
- [14] C. Poelma, *Exp. Fluids* **58**, 3 (2017).
- [15] J. J. Stickel and R. L. Powell, *Annu. Rev. Fluid Mech.* **37**, 129 (2005).
- [16] F. Boyer, É. Guazzelli, and O. Pouliquen, *Phys. Rev. Lett.* **107**, 188301 (2011).
- [17] P. Costa, F. Picano, L. Brandt, and W.-P. Breugem, *Phys. Rev. Lett.* **117**, 134501 (2016).
- [18] R. T. Cerbus, C.-c. Liu, G. Gioia, and P. Chakraborty, *Phys. Rev. Lett.* **120**, 054502 (2018).
- [19] B. Hof, C. W. H. van Doorne, J. Westerweel, and F. T. M. Nieuwstadt, *Phys. Rev. Lett.* **95**, 214502 (2005).